

## Very low sheet resistance and Shubnikov–de-Haas oscillations in two-dimensional electron gases at ultrathin binary AlN/GaN heterojunctions

Yu Cao,<sup>a)</sup> Kejia Wang, Alexei Orlov, Huili Xing, and Debdeep Jena  
*Department of Electrical Engineering, University of Notre Dame, Indiana 46556, USA*

(Received 31 December 2007; accepted 28 March 2008; published online 17 April 2008)

Very low sheet resistance two-dimensional electron gases have been obtained at ultrathin AlN/GaN heterojunctions. By investigating the molecular beam epitaxy growth conditions, the interface roughness at the heterojunction has been reduced, leading to high room-temperature electron mobilities ( $\mu \sim 1400\text{--}1600\text{ cm}^2/\text{V s}$ ) and high electron sheet densities due to spontaneous and piezoelectric polarization ( $n_s \sim 1\text{--}3 \times 10^{13}\text{ cm}^{-2}$ ) depending on the AlN thickness. This combination led to a large reduction of the room-temperature sheet resistance of  $148\ \Omega/\square$ , a new record. The improved transport properties have made it possible to observe Shubnikov–de-Haas oscillations of the magnetoresistance of the two-dimensional electron gas at ultrathin binary AlN/GaN heterojunctions for the first time. The results are indicative of the vast potential of high-quality AlN/GaN structures for a variety of device applications. © 2008 American Institute of Physics. [DOI: 10.1063/1.2911748]

The last few years have witnessed a steady march of III-V nitride heterostructure-based electronic and optical devices into realms of performance and applications that are unachievable by other semiconductor materials. Short-wavelength optoelectronic devices (light-emitting diodes and lasers) have rapidly moved from the research phase into the market. On the other hand, Al(Ga)N/GaN-based high electron mobility transistors (HEMTs) have delivered record performance characteristics for rf power amplification and are close to being commercially viable. One of the bottlenecks toward achieving very high speed operation in AlGaIn/GaN HEMTs is that the room-temperature (RT) sheet resistance  $R_{sh}$  of the two-dimensional electron gas (2DEG) channels is still above  $\sim 250\ \Omega/\square$  due to intrinsic limits set by optical phonon scattering limited mobility and polarization-induced 2DEG density. These relatively high sheet resistances hold back the performance gains that are expected by device scaling: for very short (submicron) gate lengths, they increase the parasitic access resistances<sup>1</sup> and cause electrostatic gate-length extension due to high drain voltages.<sup>2</sup> Reduction of the sheet resistance of nitride HEMTs can, therefore, lead to various performance enhancements.

Recently, it was shown that by using AlInN/AlN/GaN heterojunctions, the dc current levels in nitride HEMTs can be improved to 2.3 A/mm (from  $\sim 1.5$  A/mm for AlGaIn/GaN structures), owing to a low  $R_{sh} \sim 210\ \Omega/\square$ .<sup>3</sup> Ultrathin all-binary AlN/GaN heterojunctions, on the other hand, are ideally suited for very low sheet resistances and potentially offer the highest performance HEMTs in the III-V nitrides due to the added ease of vertical scaling for reducing short-channel effects.<sup>4</sup> Smorchkova *et al.* achieved RT sheet resistance as low as  $180\ \Omega/\square$  in such structures.<sup>5,6</sup> The theoretical limit of polarization-induced 2DEG density  $n_s$  is achieved in an AlN/GaN heterostructure:  $n_s^{\text{max}} \sim 6 \times 10^{13}\text{ cm}^{-2}$ . We recently demonstrated that it is possible to approach this limit with rf-plasma assisted molecular beam

epitaxy (MBE)-grown AlN/GaN heterojunctions. The 2DEG density was controllably tuned from  $5 \times 10^{12}$  to  $5 \times 10^{13}\text{ cm}^{-2}$  by changing the AlN barrier thickness.<sup>7</sup> A high-mobility window was observed, within which a RT  $R_{sh} \sim 170\ \Omega/\square$  was measured, the lowest in the nitrides. Furthermore, these structures were recently shown to lead to HEMTs with current densities exceeding 2 A/mm and transconductances exceeding 400 mS/mm, among the highest in nitride HEMTs.<sup>8</sup> These results clearly indicate that AlN/GaN heterostructures can exceed AlGaIn/GaN structures in a number of performance metrics. Interface roughness (IR) scattering was identified as a mobility-limiting factor in these early heterostructures<sup>7</sup> and it was indicated that improved growth conditions can enable further lowering of  $R_{sh}$ , which is the subject of this work.

The single AlN/GaN heterojunctions studied here were grown by MBE in a Veeco Gen 930 system. In this work, a high rf plasma power of 275 W was used, leading to a growth rate of  $\sim 210$  nm/h (compared to  $\sim 86$  nm/h at 150 W, as reported in Ref. 7). To maintain the growths in a metal-rich regime, high fluxes of Ga ( $\sim 1.6 \times 10^{-7}$  torr) and Al ( $\sim 1.6 \times 10^{-7}$  torr) were used. All the other growth conditions remained the same as reported earlier.<sup>7</sup> The thickness of the AlN layer was systematically varied from  $\sim 2.3$  to  $\sim 4.5$  nm, which is precisely the high-mobility window for AlN/GaN heterojunctions as identified earlier. To investigate the transport properties of 2DEGs, Hall-effect measurements were performed at RT and 77 K on Van der Pauw patterns. The measured mobilities are plotted against the 2DEG densities in Fig. 1(a). The highest mobilities achieved are  $\mu_{RT} \sim 1600\text{ cm}^2/\text{V s}$ , and  $\mu_{77\text{ K}} \sim 5900\text{ cm}^2/\text{V s}$  for  $t_{\text{AlN}} = 2.3$  nm, with  $n_s \sim 1.4 \times 10^{13}\text{ cm}^{-2}$ . The RT mobilities achieved at the higher growth rate (210 nm/h) were systematically higher than those achieved at 86 nm/h.

The higher mobilities led to a reduction of the RT sheet resistance. As shown in Fig. 1(b), the lowest  $R_{sh}$  achieved was  $148\ \Omega/\square$ , with a  $t_{\text{AlN}} = 4.0$  nm AlN cap. Hall-effect

<sup>a)</sup>Electronic mail: ycao1@nd.edu.

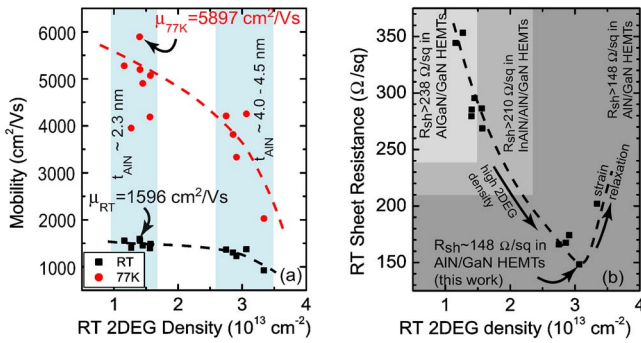


FIG. 1. (Color online) (a) Measured 2DEG  $\mu$  vs  $n_s$  at RT and 77 K for samples grown at 210 nm/h for various AlN thicknesses. (b) The resultant RT  $R_{\text{sh}}$  against the 2DEG densities for AlN/GaN 2DEGs in (a). The dashed lines are guides to the eye. The different gray scales indicate the regions of RT  $R_{\text{sh}}$  reported for AlGaN/GaN and AlInN/AlN/GaN heterostructures.

measurement on this sample showed  $\mu_{\text{RT}} = 1372 \text{ cm}^2/\text{Vs}$  and  $\mu_{77\text{K}} = 4255 \text{ cm}^2/\text{Vs}$ , with  $n_s = 3.1 \times 10^{13} \text{ cm}^{-2}$  at RT and  $2.7 \times 10^{13} \text{ cm}^{-2}$  at 77 K. The lowest sheet resistance reported in AlGaN/GaN systems is  $\sim 238 \Omega/\square$  (Ref. 9) and  $210 \Omega/\square$  in InAlN/AlN/GaN system.<sup>3</sup> Recently, a sheet resistance of  $172 \Omega/\square$  was reported with a AlN/GaN superlattice structure.<sup>10</sup> Compared to these results, the AlN/GaN structure presented here ( $R_{\text{sh}} = 148 \Omega/\square$ ) sets a new benchmark for low sheet resistances in nitride heterojunctions. It is interesting to point out that this result puts nitride heterostructures in the same category as InSb/AlInSb based heterostructure 2DEGs if low  $R_{\text{sh}}$  is the sole metric—the relatively low mobilities of nitride heterostructures compared to narrow-band gap semiconductors stemming from the high effective mass are balanced out by the extremely high polarization-induced 2DEG sheet densities achievable. The low  $R_{\text{sh}}$  is promising for pushing the performance of GaN HEMTs into current, power, and speed levels currently unachievable in AlGaN/GaN, and even AlInN/AlN/GaN heterostructures [Fig. 1(b)].

For further improvements, it is instructive to pin point the reasons for the lowering of the sheet resistance. As was shown earlier,<sup>7</sup> the electron mobility at the AlN/GaN interface is limited by polar optical phonon (POP) scattering at RT and IR scattering at low temperature. Acoustic phonon (AP) scattering is as important as IR scattering at RT, though their roles are dwarfed by POP scattering. However, since POP and AP scatterings are *intrinsic*, a marginal improvement in electron mobility (and, consequently, lower sheet resistance) is expected by lowering the IR scattering rate, which can be realized by improving the AlN/GaN interface during growth. It is difficult to quantitatively characterize the roughness of the AlN/GaN interface by microscopic techniques, however, roughness parameters may be extracted from transport measurements. To nondestructively estimate the interface quality, temperature-dependent Hall-effect measurement, combined with a theoretical model, is employed. In Fig. 2, the measured temperature-dependent mobilities are shown for two samples—one grown at a slow growth rate of 86 nm/h and the other at 210 nm/h, with  $t_{\text{AlN}} = 4.0$  and 2.3 nm, respectively. The 2DEG densities in these two samples are  $3.56 \times 10^{13}$  and  $1.13 \times 10^{13}$  at RT due to the different barrier thickness. Also shown are the theoretically calculated scattering rates due to six scattering mechanisms: POP, AP, IR, dislocations—both charge and strain-related

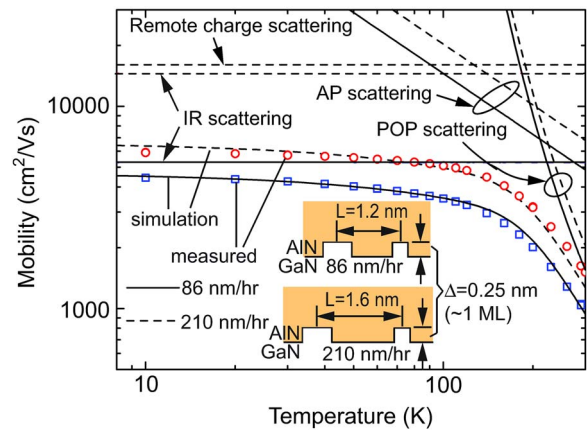


FIG. 2. (Color online) Measured temperature-dependent Hall-effect 2DEG mobility and calculations of various scattering mechanisms with a fit to the measured data for two structures. The inset shows the fitted IR model indicating that the sample grown at a higher growth rate has a larger correlation length at the AlN/GaN interface, or a smoother interface.

scattering of density  $N_{\text{disl}} \sim 10^9 \text{ cm}^{-2}$ , background impurities ( $N_{\text{imp}} \sim 10^{16} \text{ cm}^{-3}$ ), and remote Coulomb scattering (RCS) due to charged (surface) states ( $N_{\text{surf}} \sim n_s$  by charge neutrality).

By applying Matheissen's rule to the individual scattering mechanisms, the total electron mobility was calculated. In the sample grown at 210 nm/h, due to the extremely thin AlN barrier, RCS is found to be comparable to IR scattering (Fig. 2). Other Coulombic scattering mechanisms were found to be much weaker than POP, IR, and AP scattering. The IR scattering rate is evaluated using two length scale parameters—the roughness perpendicular to the interface plane ( $\Delta$ ) and an in-plane correlation length  $L$ , as indicated in Fig. 2. This figure shows the contributions from individual scattering mechanisms, the calculated total electron mobilities, and the measured mobilities from 10–300 K. The only fitting parameters are related to IR scattering and, therefore, an estimate of the roughness can be obtained by fitting the calculated data to the measured values. This yielded  $\Delta = 0.25 \text{ nm}$  ( $\sim 1 \text{ ML}$ ) and  $L$  increased from 1.2 nm for the sample grown at low growth rate (86 nm/h) to 1.6 nm for the sample grown at 210 nm/h, clearly indicating that a higher growth rate resulted in a smoother heterointerface and, therefore, a higher mobility at all temperatures. The small improvement at RT is enough to lower the RT sheet resistance and is the reason for the new record.

A clear signature of a high-quality 2DEG is quantum oscillations of longitudinal magnetoresistance at low temperatures and high magnetic fields, the Shubnikov-de Haas (SdH) effect. In addition to providing proof of the high quality of the 2DEG, SdH oscillations can provide valuable information about the sub-band occupation. Magnetotransport measurements were performed on a 2DEG sample which was grown at a low growth rate (86 nm/h). The sample had  $\mu_{\text{RT}} \sim 1460 \text{ cm}^2/\text{Vs}$  and  $\mu_{77\text{K}} \sim 4900 \text{ cm}^2/\text{Vs}$ , and  $n_s \sim 1.45 \times 10^{13} \text{ cm}^{-2}$  at RT and  $n_s \sim 1.38 \times 10^{13} \text{ cm}^{-2}$  at 77 K, measured by traditional low-field Hall effect. For high-field magnetotransport measurements, Hall bars were processed and Ohmic contacts were formed, as shown in Fig. 3(a). The sample was placed in a He low-temperature cryostat with a base temperature of 0.3 K. Magnetic fields ranging from 0 to 8 T were applied. Longitudinal ( $R_{xx}$ ) and transverse

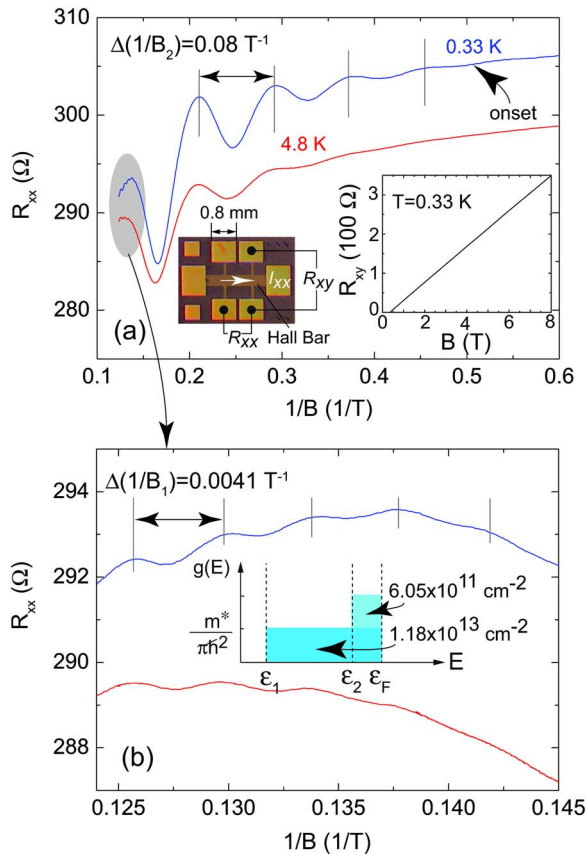


FIG. 3. (Color online) (a) Measured  $R_{xx}$  vs  $1/B$  at 0.33 and 4.8 K; the insets show measured  $R_{xy}$  vs  $B$  and optical microscope image of the Hall bar used for the measurements. (b) The second set of oscillations due to the first sub-band. The inset shows the two-sub-band occupation in the AlN/GaN heterojunction.

( $R_{xy}$ ) magnetoresistances were measured in the geometry in Fig. 3(a). The measured  $R_{xx}$  curves at 0.33 and 4.8 K are plotted against  $1/B$  and the inset shows the measured  $R_{xy}$  at  $T=0.33$  K. Clear SdH oscillations were observed in  $R_{xx}$  for the first time in binary AlN/GaN heterojunctions. Since  $\mu_{77\text{ K}} \sim 5000 \text{ cm}^2/\text{V s}$ , the onset of the oscillations is expected at a magnetic field  $B_0 > 1/\mu \sim 2$  T, which is the case in Fig. 3(a). The measured  $R_{xy}$ , with respect to  $B$ , can be used to calculate the total 2DEG sheet density in the AlN/GaN heterojunction using the relation  $n_s = B/eR_{xy} \sim 1.4 \times 10^{13} \text{ cm}^{-2}$ , in excellent agreement with the low-field Hall-effect measurement result. The oscillations of  $R_{xx}$  are periodic in  $1/B$ . The oscillatory component  $\Delta R_{xx}$  is given by<sup>11</sup>

$$\Delta R_{xx}^{\text{osc}} = \frac{\chi}{\sinh(\chi)} e^{-\pi/\mu B} \left( \frac{eB}{2\pi\hbar n_s} \right)^{1/2} \cos\left( \frac{2\pi^2 \hbar n_s}{eB} \right), \quad (1)$$

where  $\chi = 2\pi^2 k_B T / \hbar \omega_c$ ,  $\omega_c = eB/m^*$  is the cyclotron frequency,  $k_B$  is the Boltzmann constant, and  $\hbar$  is the reduced Planck's constant. The period of the oscillations in Fig. 3(a)

$\Delta(1/B_2) = 0.08 \text{ T}^{-1}$  gives a direct measurement of 2DEG density  $n_{s2} \sim 6 \times 10^{11} \text{ cm}^{-2}$  using Eq. (1). This value, however, is much lower than the  $R_{xy}$ - and Hall-effect measurement ( $n_s \sim 1.4 \times 10^{13} \text{ cm}^{-2}$ ). Interestingly, a *second* set of oscillations were observed at high fields; these oscillations are circled in Fig. 3(a) and magnified in Fig. 3(b). This second set of SdH oscillations are also periodic in  $1/B$  and yield a 2DEG density  $n_{s1} = 1.18 \times 10^{13} \text{ cm}^{-2}$  by using  $\Delta(1/B_1) = 0.0041 \text{ T}^{-1}$ . This clearly indicates the occupation of two sub-bands: ( $n_{s1}, n_{s2}$ ) represent the 2DEG densities in the first and second sub-bands, respectively. The total 2DEG density  $n_s = n_{s1} + n_{s2} \sim 1.24 \times 10^{13} \text{ cm}^{-2}$  is consistent with the values from low-field and  $R_{xy}$  measurements. Using an electron effective mass  $m^* = 0.2m_0$ , the sub-band separation  $\varepsilon_2 - \varepsilon_1$  and the Fermi level  $\varepsilon_F$  can be precisely measured by using  $n_{si} = m^*(\varepsilon_F - \varepsilon_i) / \pi \hbar^2$ , where  $\varepsilon_i$  is the  $i^{\text{th}}$  sub-band energy. This yields  $\varepsilon_F - \varepsilon_2 \sim 7.2 \text{ meV}$  and a sub-band separation  $\varepsilon_2 - \varepsilon_1 \sim 133 \text{ meV}$ . Therefore, the second sub-band is very shallow and most electrons in the 2DEG at this AlN/GaN heterojunction reside in the first sub-band, as indicated in Fig. 3(b).

In conclusion, by the optimization of rfMBE growth conditions, record low  $R_{sh}$  2DEGs at AlN/GaN heterojunctions have been obtained. Comparison of experimental temperature-dependent transport properties with a theoretical model indicates that improved heterointerface smoothness is the cause behind the improvement in mobility. The observed SdH oscillations prove two-sub-band occupation, as well as the high quality of 2DEGs at the AlN/GaN heterojunction. The results highlight the vast potential of alloy-free binary AlN/GaN heterojunctions for device applications.

The authors would like to acknowledge financial support from DARPA (Dr. M. Rosker) for this work.

<sup>1</sup>Nidhi, T. Palacios, A. Chakraborty, S. Keller, and U. K. Mishra, *IEEE Electron Device Lett.* **27**, 877 (2006).

<sup>2</sup>N. Pala, Z. Yang, A. Koudymov, X. Hu, J. Deng, R. Gaska, G. Simin, and M. S. Shur, *Proceedings of the IEEE DRC Technical Digest*, 2007 (unpublished), pp. 43–44.

<sup>3</sup>F. Medjdoub, J.-F. Carlin, M. Gonschorek, E. Feltin, M. A. Py, D. Ducatteau, C. Gaquiere, N. Grandjean, and E. Kohn, *Tech. Dig. - Int. Electron Devices Meet.* **2006**, 1.

<sup>4</sup>M. Higashiwaki, T. Mimura, and T. Matsui, *IEEE Electron Device Lett.* **27**, 719 (2006).

<sup>5</sup>I. P. Smorchkova, S. Keller, S. Heikman, C. R. Elsass, B. Heying, P. Fini, J. Speck, and U. K. Mishra, *Appl. Phys. Lett.* **77**, 3998 (2000).

<sup>6</sup>I. P. Smorchkova, L. Chen, T. Mates, L. Shen, S. Heikman, B. Moran, S. Keller, S. P. DenBaars, J. Speck, and U. K. Mishra, *J. Appl. Phys.* **90**, 5196 (2001).

<sup>7</sup>Y. Cao and D. Jena, *Appl. Phys. Lett.* **90**, 182112 (2007).

<sup>8</sup>T. Zimmermann, D. Deen, Y. Cao, J. Simon, P. Fay, D. Jena, and H. Xing, *Electron Device Lett.* (to be published).

<sup>9</sup>R. Gaska, J. W. Yang, A. Osinsky, Q. Chen, M. Asif Khan, A. O. Orlov, G. L. Snider, and M. S. Shur, *Appl. Phys. Lett.* **72**, 707 (1998).

<sup>10</sup>Y. Kawakami, A. Nakajima, X. Q. Shen, G. Piao, M. Shimizu, and H. Okumura, *Appl. Phys. Lett.* **90**, 242112 (2007).

<sup>11</sup>R. Kubo, H. Hasegawa, and N. Hashitsume, *J. Phys. Soc. Jpn.* **14**, 56 (1959).